A LAXS (Large Angle X-ray Scattering) and EXAFS (Extended X-ray Absorption Fine Structure) Investigation of Conductive Amorphous Nickel Tetrathiolato Polymers

Thomas Vogt,[1] Christophe Faulmann, Régis Soules, Pierre Lecante, Alain Mosset, Paule Castan, Patrick Cassoux,* and Jean Galy

Contribution from the Laboratoire de Chimie de Coordination du CNRS, Unité No. 8241 liée par convention à l'Université Paul Sabatier, 205 route de Narbonne, 31077 Toulouse Cedex, France.
Received May 26, 1987

Abstract: The structure of amorphous partially oxidized nickel tetrathiolato polymers has been studied by EXAFS and LAXS (large angle X-ray scattering). These polymers are the following: (i) the poly(nickel ethylenetetrathiolates) with different countercations, referred to as $[(Ni\text{-}ett)Na_{0.31}]_n$ (**1a**), $[(Ni\text{-}ett)K_{0.25}]_n$ (**1b**), $[(Ni\text{-}ett)(n\text{-}Bu_4N)_{0.75}]_n$ (**1c**), and $[(Ni\text{-}ett)(Co(pmi)_2)_{0.5}]_n$ (**1d**); (ii) the poly(nickel tetrathiafulvalenetetrathiolates), $[(Ni\text{-}ttftt)Na_{0.3}]_n$ (**2a**) and $[(Ni\text{-}ttftt)(Bu_4N)_{0.5}]_n$ (**2b**); and the poly(nickel tetrathiosquarate), $[(Ni\text{-}tts)K_{0.15}]_n$ (**3**). An EXAFS study of **1a** shows that the nickel atom is surrounded by four sulfur atoms (Ni–S = 2.169 (8) Å) and four carbon atoms (Ni–C = 3.06 (1) Å). This result is the first experimental evidence, in such polymers, that ett acts as a bischelating ligand on two metal atoms. LAXS investigations of all polymers confirm this structure in the first coordination sphere and give additional information on the polymer chain packing. The studied polymers exhibit two types of structural arrangement. The packing in type I polymers (**1a**, **1b**, **1d**, **2a**, and **3**) is the most dense and consists of coplanar parallel polymer chains located in parallel planes. The chains are stacked perpendicularly to their plane and eclipsed. The interchain distances within a plane (interstack) vary between 3.7 and 4.3 Å and the interplanar stacking distances (intrastack) between 3.8 and 5.7 Å. In type II polymers (**1c** and **2b**) the chains are also stacked perpendicularly to their plane (stacking distance = 4.3–4.4 Å) but the interstack distances are much larger (>10 Å). The type of structural arrangement of a polymer is not solely determined by the nature of the tetrathiolato bridging ligand but by those of the countercation. This result can be rationalized in terms of isolobal analogy of the metal d^8 (Ni^{2+}), the ethylene (C_2^{4+}), and the squarate (C_4^{6+}) fragments. The experimental density of the polymers and their electrical conductivity are correlated with their structural arrangement.

A survey of the recent literature in chemistry shows a steady and fast increase of the number of crystal structure determinations reported for the compounds investigated. Two main reasons may account for this increase: (i) the greater availability of automatic X-ray diffractometers and related structure solving systems in research institutions and (ii) the growing need, even for synthetic chemists, to use structure–properties relationships that help in understanding these properties and designing new interesting chemical systems.

The situation looks totally different when the compound investigated is amorphous or simply badly crystallized. In such a case, even if this compound may be of great interest, further research development is frequently hindered by such a lack of structural information.

The EXAFS technique,[2] which gives valuable structural information, is now widely used (but synchrotron radiation facilities are submitted to annual schedule). This EXAFS information is, however, restricted to the first or second coordination sphere around a central atom. Another possible technique for obtaining significant information on the structural architecture of amorphous material is LAXS (Large-Angle X-ray Scattering) and has been known for a while.[3] However, the development of this technique has been limited by the time requested for collection of usable data. Following recent progress in instrumentation[4] and software,[5] the LASIP[2] system, developed in our laboratory,[5] overcomes this difficulty and makes LAXS at the experimental level almost a routine technique. This system has been successfully used for investigating inorganic polymers with extended chain structures.[6]

We report here a LAXS and EXAFS study of three different types of amorphous nickel tetrathiolato polymers (Figure 1): (i) the poly(nickel ethylenetetrathiolates) with different countercations, referred to as $[(Ni\text{-}ett)Na_{0.31}]_n$ (**1a**), $[(Ni\text{-}ett)K_{0.25}]_n$ (**1b**), $[(Ni\text{-}ett)(n\text{-}Bu_4N)_{0.75}]_n$ (**1c**), $[(Ni\text{-}ett)(Co(pmi)_2)_{0.5}]_n$ (**1d**); (ii) the poly(nickel tetrathiafulvalenetetrathiolates), $[(Ni\text{-}ttftt)Na_{0.3}]_n$ (**2a**) and $[(Ni\text{-}ttftt)(Bu_4N)_{0.5}]_n$ (**2b**); and the poly(nickel tetrathiosquarate), $[(Ni\text{-}tts)K_{0.15}]_n$ (**3**).

Polymers **1** and **2** have aroused great interest because of their high compaction powder conductivity (up to 50 $\Omega \cdot cm^{-1}$).[7,8] They have been the subject of several research works including their formation mechanism,[7-10] degree of partial oxidation, electrical conductivity,[10,11] and magnetic behavior.[10,12] In these previous works,[7-12] chemical intuition led us to think that tetrathiolate ligands such as ett or ttftt act as bischelating chelating ligands on two metal atoms (see Figure 1). Other structural hypotheses also could have been considered, such as metal chelation through two thiolato groups of the same carbon atom of the ligand ("dithiocarbamate-like") or chelation of different metal atoms by each thiolato group, ... In any case, no direct experimental evidence of their molecular structure or even of the coordination mode of the metal has been presented so far.

In polymer **1d**, the countercation is the cobalt(II) complex cation $[Co(pmi)_2]^{2+}$ (Figure 1). It is derived from $[Co(pmi)_3](BF_4)_2$,[13]

(1) Permanent address: Institut für Anorganische Chemie der Universität, Auf der Morgenstelle 18, 7400 Tübingen, FRG.

(2) Abbreviations: EXAFS, extended X-ray absorption fine structure; LAXS, large angle X-ray scattering; LASIP, liquid and amorphous structure investigation package; ett, ethylenetetrathiolate ($C_2S_4^{4-}$); pmi, 2-pyridinal methylimine; ttftt, tetrathiafulvalenetetrathiolate ($C_6S_8^{4-}$); tts, tetrathiosquarate ($C_4S_4^{2-}$); BEDT-TTF, bis(ethylenedithio)tetrathiafulvalene; H_2dmit, 4,5-dimercapto-1,3-dithiole-2-thione; TTF, tetrathiafulvalene.

(3) (a) Debye, P. *Ann. Phys. (Leipzig)* **1915**, *46*, 809–813. (b) Warren, B. E. *X-ray Diffraction*; Addison Wesley: Reading, 1969. (c) Waseda, Y. *Structure of Non-crstalline Materials: Liquids and Amorphous Solids*; McGraw Hill: New York, 1980.

(4) Galy, J.; Mosset, A.; Lecante, P. French Patent 80.16170, (ANVAR) 1980; UK Patent 2081440B, 1984; US Patent 4 475 225, 1985.

(5) Lecante, P.; Mosset, A.; Galy, J. *J. Appl. Crystallogr.* **1985**, *18*, 214–218.

(6) (a) Mosset, A.; Galy, J.; Coronado, E.; Drillon, M.; Beltran, D. *J. Am. Chem. Soc.* **1984**, *106*, 2864–2869. (b) Abboudi, M.; Mosset, A.; Galy, J. *Inorg. Chem.* **1985**, *24*, 2091–2094. (c) Vogt, T.; Mosset, A.; Strähle, J.; Galy, J. *C. R. Acad. Sci., Ser. 2* **1986**, *303*, 365–368.

(7) (a) Engler, E. M.; Nichols, K. H.; Patel, V. V.; Rivera, N. M.; Schumaker, R. R. US Patent 4 111 857, 1978. (b) Rivera, N. M.; Engler, E. M. *J. Chem. Soc., Chem. Commun.* **1979**, 184–185.

(8) Poleschner, H.; John, W.; Kempe, G.; Hoyer, E.; Fanghänel, H. *Z. Chem.* **1978**, *18*, 345–346.

(9) (a) Ribas, J.; Cassoux, P. *C. R. Acad. Sci., Ser. 2* **1981**, *293*, 665–670. (b) Vicente, R.; Ribas, J.; Cassoux, P. *Nouv. J. Chim.* **1984**, *8*, 653–658.

(10) Vicente, R.; Ribas, J.; Cassoux, P.; Valade, L. *Synth. Met.* **1986**, *13*, 265–280.

(11) Holdcroft, G. E.; Underhill, A. E. *Synth. Met.* **1985**, *10*, 427–435.

(12) Poleschner, H.; Fanghänel, E.; John, W.; Hoppe, F.; Roth, S. *J. Prakt. Chem.* **1983**, *325*, 957–975.

0002-7863/88/1510-1833$01.50/0

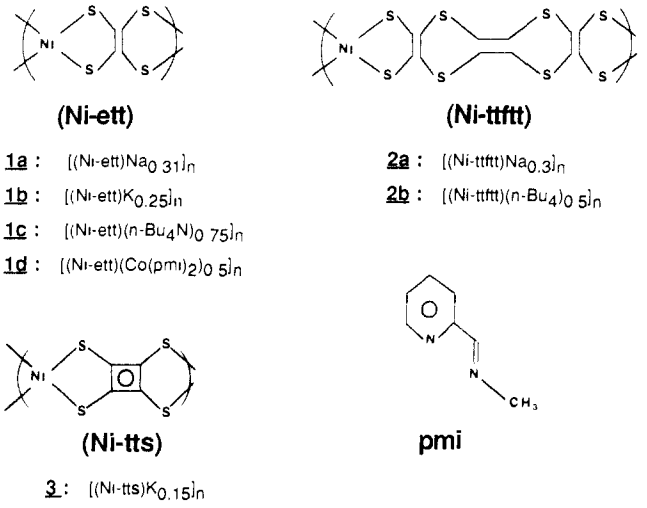

Figure 1. The (Ni-ett), (Ni-ttftt), and (Ni-tts) polymer units and the pmi ligand.

which exhibits an unusual thermally induced high-spin ↔ low-spin transition.[14] Polymer **1d** was obtained while investigating[15] the feasibility of transferring this interesting magnetic behavior to conductive polymer chains.

Polymers of type **3** are derived from the tetrathiosquarate ligand. Transition-metal compounds of this ligand, and of squarate and dithiosquarate as well, have also appeared as a source of materials with interesting physical properties.[16-19] The coordination mode in some of these compounds may also be questioned. A ribbon chain structure, with the tetrathiosquarate dianion acting as a bridging bischelate ligand, has been proposed for the nickel and palladium tetrathiosquarato complex,[18] but no crystal structure has been experimentally determined so far. In the crystal structures of potassium bis(dithiosquarato)nickelate and -palladate, the sulfur atoms are chelating the nickel and palladium atoms.[19a,b] Further, in the structure of the nickel squarate dihydrate, each squarate oxygen atom is bonded to a different nickel atom.[20a] Likewise, in the structure of $[Ce_2(H_2O)_{10}(C_4O_4)][Ni(S_2C_2O_2)_2]_2 \cdot 5.2H_2O$, each squarate oxygen atom is bonded to a different cerium atom.[20b]

Experimental Section

Synthesis. Polymers **1a** and **1c** have been prepared as previously described.[10] Polymer **1b** has been obtained following the method described for polymer **1a**, but substituting in this procedure potassium to sodium.

Polymer **1d** has been prepared in a similar way. 1,3,4,6-Tetrathiapentalene-2,5-dione[21] was reacted with sodium methoxide (4 mol equiv) in refluxing methanol for 2-3 h. To the resulting solution, $Ni(acac)_2$ (1 mol equiv) was added and the solution was refluxed for 12 h. The resulting dark solution was filtered in order to eliminate any trace of solid impurities and a methanolic solution of $[Co(pmi)_3](BF_4)_2$[13] (1 mol equiv) was added. A black powder precipitated immediately and was collected by filtration, washed with methanol, water, and acetone, and dried under vacuum. All the reactions were carried out under inert atmosphere. The results of the elemental analysis (Anal. Calcd for $C_9H_8Co_{0.5}NiN_2S_4$: C, 29.97; H, 2.22; Co, 8.18; Ni, 16.29; N, 7.77. Found: C, 28.48; H, 2.09; Co, 6.08; Ni, 12.70; N, 6.68) and of TGA measurements[15] show the presence of solvent molecules. However, the ratios Co/Ni and N/Co are close to 0.5 and 2, respectively, indicating the formula [(Ni-ett)(Co(pmi)$_2$)$_{0.5}$], which implies the loss of one pmi ligand per cobalt atom.

Polymers **2a** and **2b** have been prepared as previously described.[9a]

Polymer **3** has been prepared as follows. An aqueous solution of $NiCl_2$ (0.047 mg in 5 mL) was added to an aqueous solution of potassium tetrathiosquarate (0.1 g in 5 mL). A red precipitate separated immediately and the mixture was stirred for 30 min and filtered off. Upon

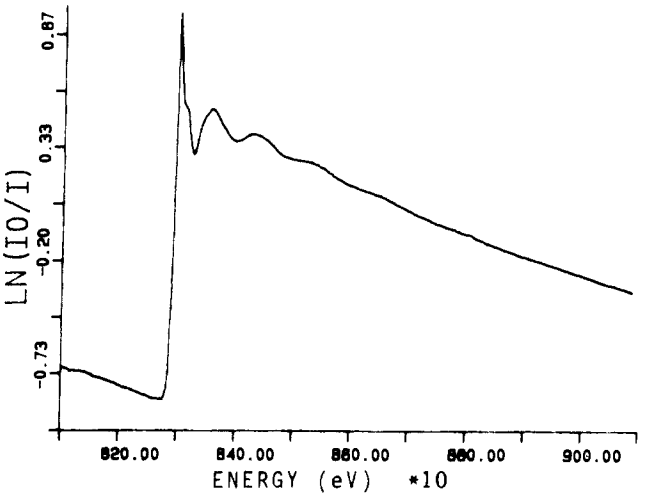

Figure 2. EXAFS absorption spectrum of polymer **1a**.

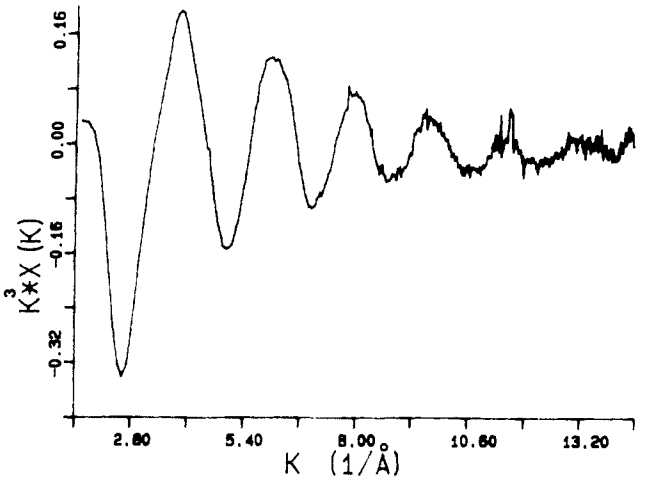

Figure 3. Weighted $k^3 \times \chi(k)$ curve in the k-space for polymer **1a** ($k = 4\pi \sin\theta/\lambda$).

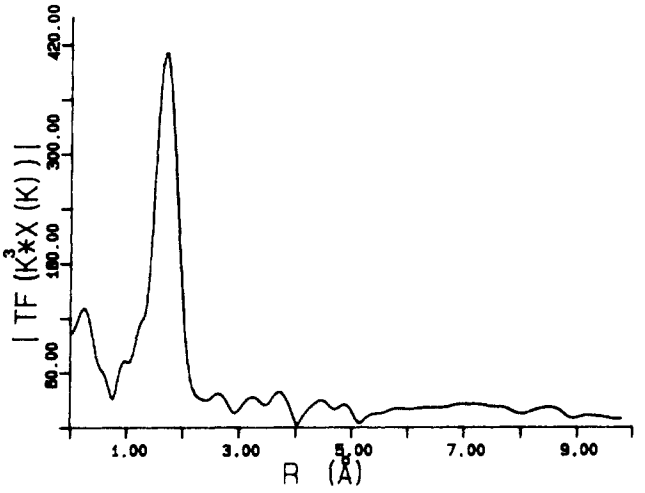

Figure 4. EXAFS radial distribution curve of polymer **1a**.

(13) Figgins, P. E.; Busch, D. H. *J. Am. Chem. Soc.* **1960**, *82*, 820-824.
(14) Stoufer, R. C.; Smith, D. W.; Clevenger, E. A.; Norris, T. E. *Inorg. Chem.* **1966**, *5*, 1167-1171.
(15) Thuery, P.; Kahn, O.; Faulmann, C.; Cassoux, P., unpublished results.
(16) (a) Cohen, S.; Lacker, J. R.; Park, J. D. *J. Am. Chem. Soc.* **1959**, *81*, 3480-3485. (b) West, R.; Niu, H. Y.; Powel, D. L.; Evans, M. V. *Ibid.* **1960**, *82*, 6204.
(17) (a) Böhm, M. C. *Physica* **1983**, *112B*, 302-314; (b) *Ibid.* **1984**, *124B*, 327-351; (c) Böhm, M. C. *Phys. State Solid (b)* **1984**, *121*, 255-264.
(18) Götzfried, F.; Beck, W.; Lerf, A.; Sebald, A. *Angew. Chem., Int. Ed. Engl.* **1979**, *18*, 463-464.
(19) (a) Coucouvanis, D.; Holah, D. G.; Hollander, F. J. *Inorg. Chem.* **1975**, *14*, 2657-2665. (b) Bonnet, J.-J.; Cassoux, P.; Castan, P.; Laurent, J.-P.; Soules, R. *Mol. Cryst. Liq. Cryst.*, in press.
(20) (a) Habenschuss, M.; Gerstein, B. C. *J. Chem. Phys.* **1974**, *61*, 852-860. (b) Trombe, J.-C.; Gleizes, A.; Galy, J. *C. R. Acad. Sci., Ser. 2* **1986**, *302*, 21-24.
(21) Schumaker, R. R.; Engler, E. M. *J. Am. Chem. Soc.* **1977**, *99*, 5521-5522.

Table I. Standard EXAFS Parameters[23] Calculated for Polymer **1a**[a]

interaction	N	σ	γ (Å^{-1})	R (Å)	ΔE_0 (eV)
Ni–S	4	0.073 603	0.125	2.169	−15.175
Ni–C	4	0.089 978	0.125	3.056	−15.175

[a] N, number of neighbors; σ^2, mean-squares deviation for a Gaussian distribution of R; $\gamma = 1/\lambda$, inverse of the photoelectron free mean-path; ΔE_0, shift of the threshold energy.

subsequent treatment and whatever the conditions (washing with ethanol or not, working under inert atmosphere), the precipitate darkened upon drying and finally turned black and lustrous. The same observation was made when preparing this compound in nonaqueous solvents such as acetonitrile. Anal. Calcd for $C_4S_4NiK_{0.15}\cdot H_2O$: C, 18.57; H, 0.77; Ni, 22.70; K, 2.26. Found: C, 19.26; H, 0.56; Ni, 22.43; K, 2.43.

EXAFS Studies. The EXAFS spectrum of polymer **1a** was measured at LURE-CNRS (Université de Paris-Sud, Orsay) on the DCI EXAFS III spectrometer described by Raoux et al.,[22] using a Si 211 channel-cut monochromator. Before the sample was measured, a Ni base line was registered and used to correct the spectrum afterwards. Figure 2 shows the obtained absorption spectrum. These data were analyzed by using the EXAFS formula for the phase wave approximation and the theoretical amplitude and phase shifts by Teo et al.[23] The details of data analysis have been previously described.[24] The transformation in the k-space led to the weighted $k^3 \times \chi(k)$ curve shown in Figure 3. The Fourier transformation of $k^3 \times \chi(k)$ from k- to R-space gave the radial distribution curve (Figure 4) in which each shell is represented by a peak.

LAXS Studies. The polymers were carefully ground and pressed (200 kg/cm^2) into 0.2–0.3 mm thick pellets. They were mounted on a goniometer head and the diffuse spectra scattered by the samples irradiated with graphite-monochromatized molybdenum Kα radiation (λ = 0.71069 Å; Mo X-ray tube power, 1125 W) were obtained with an ω–θ goniometer equipped with a linear position-sensitive detector (LPSD).[4,5] The pellets were oriented perpendicular to the X-ray beam when the goniometer angles were at zero. Scattered intensities were measured with the θ–2θ scan mode. The Bragg angle covered by the LPSD is $2\theta = 12°$. The integration of erratic data due to the detector wire requires that the LPSD sweeps across the whole 2θ area under investigation. Each detector channel successively proceeds before each measuring point of the 2θ domain. Some 2200 equidistant points were measured typically in 22 h with $3° < 2\theta < 132°$.

All the data processing was carried out on a VAX 11/730 with the LASIP system and have been detailed elsewhere.[5] The scattered intensities were corrected for polarization and absorption effects, normalized by comparison with the sum of coherent and incoherent independent intensities with the methods of Krogh-Moe and Burian et al.[25] The atomic scattering factors for the Ni, C, and S atoms were taken from Cromer and Waber,[26] and Compton diffusion factors were from Cromer.[27]

The experimental radial distribution function, $F(r)$, which shows the distribution of the interatomic distances in the polymers, is obtained by using the Zernicke and Prins relation.[28] The theoretical radial distribution function, $F(r)_{theor}$, is calculated for structural models by the Fourier transform of Debye's formula of theoretical intensities.[3a]

Density and Conductivity Measurements. The density of the polymers has been measured by the flotation method in tetrabromoethane/ethanol. The compaction conductivities of powdered samples of the polymers were estimated on compressed pellets with a Wayne-Kerr Model B605 automatic component bridge.

Results

EXAFS Investigation of Polymer 1a. The EXAFS radial distribution curve of polymer **1a** (Figure 4) shows one strong peak and no direct evidence of further interactions. This suggests that this peak results at the most from two types of short distance interactions, Ni–S and Ni–C. Longer Ni–S interactions are not observed, probably because of the single-electron/single-scattering approximation used in the EXAFS formula. Multiple scattering

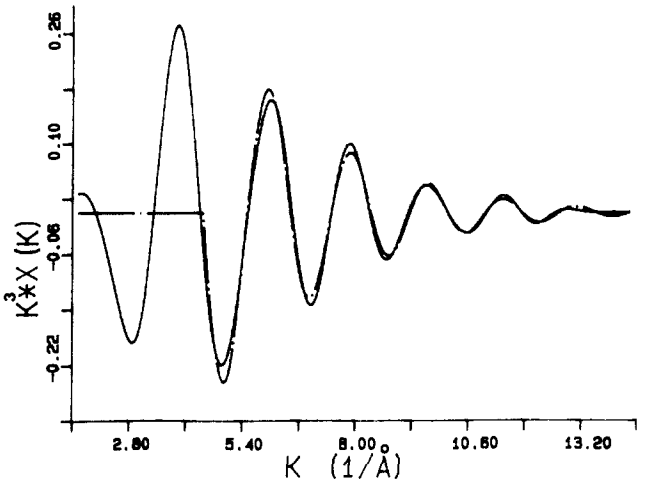

Figure 5. Best fit obtained for polymer **1a**: (—) experimental $k^3 \times \chi(k)$ curve; (- - -) theoretical $k^3 \times \chi(k)$ curve.

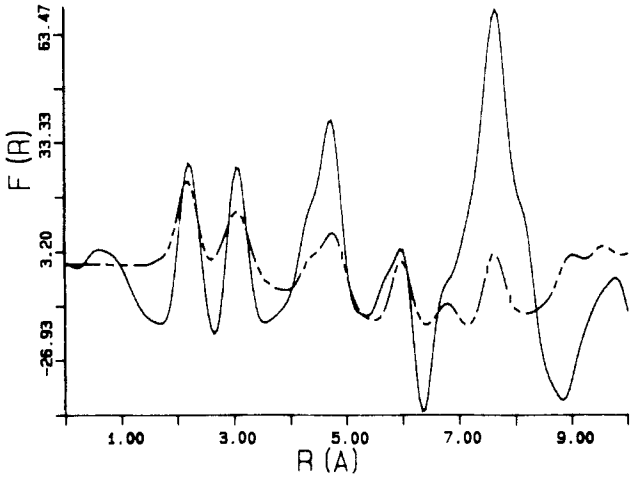

Figure 6. Experimental RDF curve (—) of polymer **1a** and theoretical RDF curve (- - -) calculated for a single-chain model.

and other phenomena described by Lee et al.[29] and Hayes et al.[30] set an upper limit between 3 and 5 Å^{-1} in the k-space. It is possible that low-temperature EXAFS spectra could exhibit longer range interactions: at 30 K, the spectra of copper(II) μ-oxalato chains do show intermolecular interactions due to the reduced thermal vibrations of less strongly coupled Cu–Cu pairs, which are not observed at 300 K.[31]

Standard EXAFS parameters were determined through various simulation and curve fitting by nonlinear least-squares refinement[32] and are listed in Table I. Figure 5 shows the best fit obtained with these parameters. The agreement between theoretical and experimental data is satisfactory (least-squares deviation is 2%).

EXAFS Calculation. It should be noted that this result is the first direct physical evidence that in the considered polymers the nickel atom is surrounded by four sulfur atoms and four carbon atoms, thus confirming the suggested coordination mode and structure shown in Figure 1. With Ni–S = 2.169 (8) Å and Ni–C = 3.06 (1) Å, and assuming a C–S bond length of 1.75 Å,[33] reasonable values for C–C = 1.35 Å, S–Ni–S = 95°, and Ni–S–C = 103° may be calculated.

LAXS Investigation of Polymer 1a. With this information at hand, a single-chain structural model (Figure 6) can be used in a first stage for fitting, by using the computer programs included

(22) Raoux, O.; Petian, J.; Bandot, P.; Galais, G.; Fontaine, A.; Lagarde, P.; Levitz, P.; Laipias, G.; Sadoc, A. *Rev. Phys. Appl.* **1980**, *15*, 1079–1084.
(23) Teo, B. K.; Lee, P. A.; Simons, A. L.; Eisenberg, P.; Kincaid, B. M. *J. Am. Chem. Soc.* **1977**, *99*, 3854–3856.
(24) Michailowicz, A.; Huet, J.; Gaudemer, A. *Nouv. J. Chim.* **1982**, *6*, 79–84.
(25) (a) Krogh-Moe, J. *Acta Crystallogr.* **1956**, *9*, 951–953. (b) Burian, A.; Rzepa, B.; Lecante, P.; Mosset, A. *J. Mat. Sci. Lett.* **1985**, *4*, 701–703.
(26) Cromer, D. T.; Waber, J. T. *International Tables for X-ray Crystallography*; Kynoch Press: Birmingham, 1974; Vol. IV.
(27) Cromer, D. T. *J. Chem. Phys.* **1969**, *50*, 4857–4859.
(28) Zernicke, F.; Prins, J. A. *Z. Phys.* **1927**, *41*, 184–187.
(29) Lee, P. A.; Citrin, P. H.; Eisenberger, P.; Kincaid, B. M. *Rev. Mod. Phys.* **1981**, *53*, 764–770.
(30) Hayes, T. M.; Boyce, J. B. *Solid State Phys.* **1982**, *37*, 173–177.
(31) Verdaguer, M.; Julve, M.; Michailowicz, A.; Kahn, O. *Inorg. Chem.* **1983**, *22*, 2624–2629.
(32) James, F.; Roos, M. *Computer Phys. Commun.* **1975**, *10*, 345–367.
(33) *Molecular Structures and Dimensions*; Kennard, O., Ed.; N.V.A. Dosthocks Witgewers Mij; Utrecht, 1972; Vol. A1.

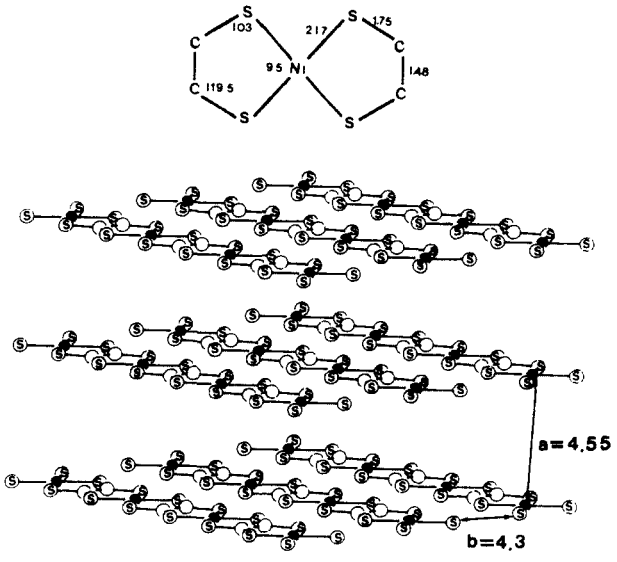

Figure 7. ORTEP drawing of the nine-chain model of polymer **1a**.

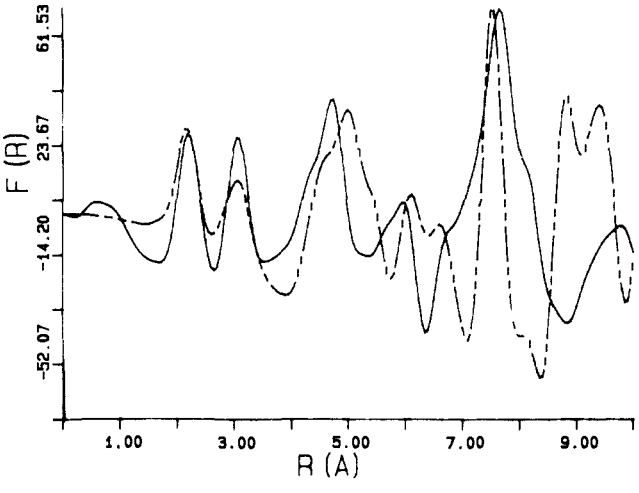

Figure 8. Experimental RDF curve (—) of polymer **1a** and theoretical RDF curve (- - -) calculated for the nine-chain model shown in Figure 7.

in the LASIP system,[5] the experimental LAXS RDF curve of polymer **1a**. As shown in Figure 6, the first calculated peak is in good agreement, as for position and intensity, with its experimental counterpart. The position of the other peaks also fits well, but the intensities are quite different, especially at $R \cong 4.5$ and 7.5 Å. This shows that the single-chain model is not sufficient to explain all the features of the experimental RDF curve and suggests that interchain interactions must be taken into account. A similar problem has been encountered previously in the case of amorphous transition-metal rubeanates.[6b]

Interchain interactions were introduced by using multi-chain models built up with several single-chain models placed at different positions and having different orientations. From over eighty simulations, the nine-chain model shown in the ORTEP drawing of Figure 7 can be proposed. It consists of three parallel planes each containing three coplanar parallel polymer chains. Within a plane, the interchain S···S distance is 4.3 Å. The polymers are stacked perpendicularly to their plane and eclipsed. The stacking Ni···Ni distance is 4.55 Å, i.e., somewhat larger than those observed in related conducting molecular complexes such as $(NBu_4)_{0.29}[Ni(dmit)_2]$ (≈3.77 Å)[34a] and $TTF[Ni(dmit)_2]_2$ (3.73 Å).[34b] This nine-chain model gives the closest approach to the

(34) (a) Valade, L.; Legros, J.-P.; Bousseau, M.; Cassoux, P.; Garbauskas, M.; Interrante, L. V. *J. Chem. Soc., Dalton Trans.* **1985**, 783–793. (b) Bousseau, M.; Valade, L.; Legros, J.-P.; Cassoux, P.; Garbauskas, M.; Interrante, L. V. *J. Am. Chem. Soc.* **1986**, *108*, 1908–1916.

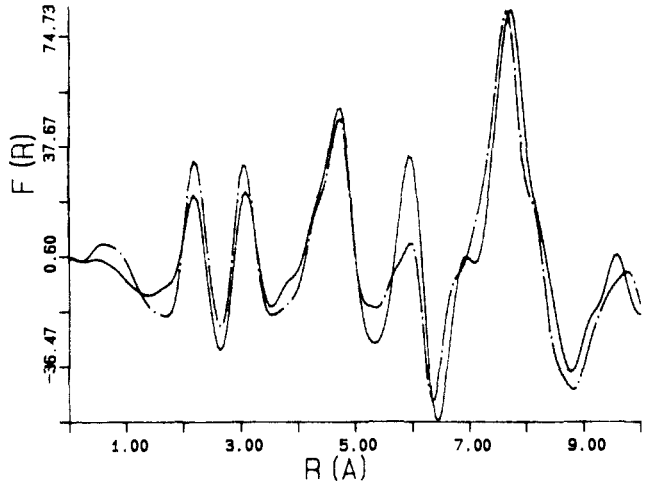

Figure 9. Comparison of the experimental RDF curves of polymer **1a** (-·-) and polymer **1b** (—).

experimental data as shown in Figure 8. The agreement observed in the 7.5-Å range can be taken as an indicator for the reliability of this model. However, it should be kept in mind that the Na^+ counterions and residual solvent molecules are not taken into account and this may explain some of the discrepancies observed in Figure 8. Moreover the nine-chain model yields two intense theoretical peaks at ≈9 Å which are not observed in the experimental RDF curve. This may be explained by two factors. The first one results from the quasicrystalline model used in such fits. Such a model is too rigid and leads to emphasize long-range interactions which may exist in the amorphous material with a higher dispersion in their distances. For example, in the stacking arrangement of the model of **1a** each atom of a chain corresponds to a homologous atom at ≈9 Å. In the actual amorphous material, the stacking is probably much less regular and this should lead to the weakening of the corresponding peak. Another explanation for this discrepancy may be related to the use of a pseudo temperature factor in the calculation of the RDF curve.[5] This temperature factor depends only on the nature of the atoms involved, and it is clear that it should be different for short- and long-range interactions.

LAXS Investigation of Polymer 1b. Several attempts were made, but without success, to locate the Na^+ countercations in polymer **1a**. This led us to investigate polymer **1b** in which the Na^+ cation is replaced by the K^+ cation. By doing so, it was hoped that changes in the RDF curve would yield some footprints. Figure 9 shows a comparison of the experimental RDF curves of polymers **1b** and **1a**. It can be seen that both curves are almost identical with the exception of the increase of the intensity of the peak at ca. 6 Å in the case of polymer **1b**. We have found no explanation for this variation, but it may be due to the influence of the chain length. In any case, all subsequent attempts to locate the K^+ cations in the model structure have failed. Nevertheless, these simulations and the close analogy between the RDF curves of **1a** and **1b** show that the same model used for **1a** also fits the data obtained for **1b**.

LAXS Investigation of Polymers 2a and 3. The studies on polymers **2a** and **3** were engaged in order to evaluate the influence of the size and nature of the ligand on the structure of these polymers. In **2a**, the ligand ttftt is a much larger tetrathiolate system than the ett ligand of **1a** and **1b**. In **3**, the nature of the tts ligand is even more different.

A comparison of the experimental RDF curves of **1a** and **2a** is shown in Figure 10. Both curves are strikingly similar. Hence again, a nine-chain model similar to that used for **1a** (Figure 7) should also fit the experimental RDF curve of **2a**. This was confirmed by using such a model for calculating the theoretical RDF curve: the first peak indicated a Ni–S distance of 2.17 Å. The second peak could be fitted satisfactorily by various internal geometries of the single-chain unit. The only way to select the appropriate one was by fitting simultaneously the internal geom-

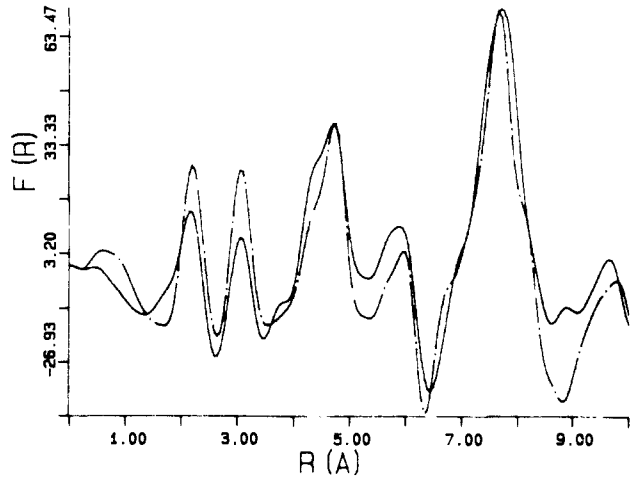

Figure 10. Comparison of the experimental RDF curves of polymer **1a** (-·-) and polymer **2a** (—).

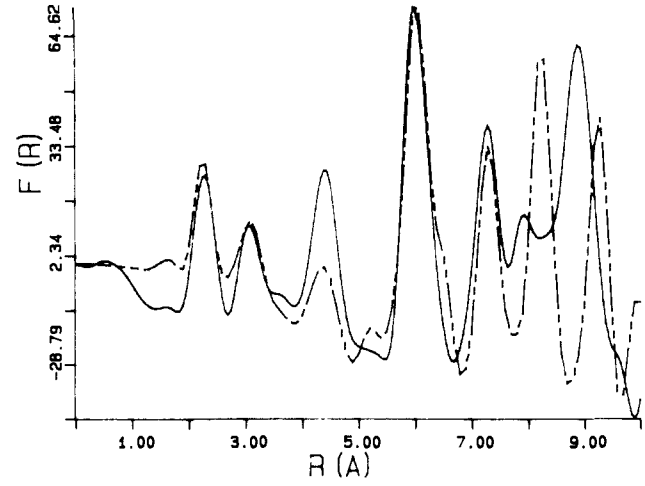

Figure 11. Experimental RDF curve of polymer **2a** (—) and theoretical RDF curve (---) calculated by using the structural model of Figure 12.

etry of the single-chain unit of **2a** *and* the stacking arrangement of these units in the nine-chain model. Due to the complexity of the ttft ligand, the final geometry which gives the best fit is a compromise resulting from *intra-* and *inter*-chain interactions. However, since such simulations make no difference between bonding and nonbonding interactions, the peak intensities derived from the calculations may deviate from the experimental ones. Moreover, in the quasicrystalline models used in such fits, the polymer chain is supposed to be strictly planar, when, as a consequence of a statistical disorder of the atoms around this ideal plane, the actual geometry of the chain may deviate from planarity. We have previously made a similar observation in the case of the (μ-pyrazolato)$_3$Mo^{III}.[6c] In the same way, the larger intensity of the second theoretical peak at ca. 3 Å compared to the intensity of the corresponding experimental peak may be corrected by assigning different values to the dispersion parameter, l_{ij}, affecting the interatomic distances in the Debye's formula[3a] for bonding and nonbonding interaction. For a large polymer such as **2a**, such intricate and somewhat arbitrary corrections should not bring a really profitable improvement to the best fit shown in Figure 11 and obtained by using the quasicrystalline nine-chain model described in Figure 12.

The tetrathiosquarate polymer **3** exhibits an experimental RDF curve (Figure 13) that resembles those of polymers **1a**, **1b**, and **2a**. However, if the positions of the main peaks are similar, their intensities are different. For example, the most intense peak in the RDF curve of **3** is now observed at ≈6 Å. The first two peaks alone allow for fixing the geometry of the (Ni-tts) unit, since they stem from Ni–S, Ni–C, and S–S interactions within the polymer chain and are not perturbed by interchain interactions. The first peak at 2.25 Å corresponds to four Ni–S interactions. This value for the Ni–S bond length in **3** compares well with Ni–S distances in similar NiS_4 systems: 2.185 Å in the $Ni(S_4)_2^{2-}$ anion;[35] 2.234 and 2.212 Å in $K_2Ni(S_2C_4O_2)_2\cdot 2H_2O$.[19a] The S–Ni–S angle (93°) and the C–S bond length (1.65 Å) were calculated by fitting the second peak which originates mainly from the Ni–C and S–S interactions, while preserving an idealized geometry for the squarate unit with all angles fixed at 90° and C–C bond lengths at 1.45 and 1.46 Å. It may be noted that the calculated S–Ni–S angle compares well with the experimental value of this angle in $K_2Ni(S_2C_4O_2)_2\cdot 2H_2O$ (93° vs 94.19°[19a]). Figure 13 shows the best theoretical fit that could be obtained and Figure 14 shows the nine-chain model used in this fit. Direct determination of the C–S distance from the RDF was not possible. Due to the scattering factors of the C and S atoms, the corresponding peak is weakened and perturbed by the C–C interactions. The weak shoulder observed on the left side of the Ni–S peak at 2.25 Å is due to these small contributions. The tetrathiosquarate ligands were considered as individually planar, and coplanar within the chain. This approximation is consistent with the crystal structure of $K_2Ni(S_2C_4O_2)_2\cdot 2H_2O$ in which the dihedral angle between the tetrathiosquarate planes is 1.22°.[19a] Such a small distortion falls into the error range of the LAXS technique. Finally, it should be noted that the stacking distance in **3** (5.7 Å) is much larger than that in **1a** and **2a**.

LAXS Investigation of Polymers 1c, 1d, and 2b. The studies on these three polymers were carried out in order to evaluate the influence of the size of the countercation. The experimental RDF curves of polymers **1c** and **2b** (Figure 15) exhibit striking similarities. Therefore, as previously observed when comparing the data for polymers **1a** and **2a**, changes in the size of the tetrathiolate ligand (i.e., going from ett to ttftt) do not result in appreciable changes in the overall structural arrangement of polymers **1c** and **2b**.

By contrast, these experimental RDF curves are quite different from those of polymers **1a** and **2a** (Figure 10), especially for interactions larger than 3.5 Å, indicating that the structural arrangement is quite different. Actually, it was not possible to fit the data of polymer **1c** when using the nine-chain model obtained for polymer **1a**. The best theoretical RDF curve was obtained for **1c** (Figure 16) when using the three-chain structural model shown in Figure 17. This model consists of three polymer chains stacked perpendicularly to their plane. Each stack is isolated and more than 10 Å apart from any other stack. It was impossible to fit satisfactorily the peaks at 6 and 9 Å when using models in which the polymer chains are strictly eclipsed. The best fit shown in Figure 16 was obtained by introducing a slight slipping of the chains shown in Figure 17. This slipping is characterized by a β angle of 6.5° between the Ni–Ni interchain interaction and the perpendicular to the plane of the chain. The stacking in **1c** may be consequently described as roof-tile-like. The Ni–Ni spacing is 4.4 Å, but the interchain distance is 4.37 Å. This type of "slipped" stacking is very common in transition-metal complexes with sulfur-containing planar ligands.[34,36,37] In many cases, the stacked molecules are surrounded by non-interacting cations. Hoffmann et al.[38] have predicted that the interaction of the four π lone-pair orbitals in stacked metal complexes with sulfur-containing ligands induces a slipping from the eclipsed stacking which is energetically favored only if partially filled HOMO's are considered with an opposite contribution of the metal d_{z^2} and d_{xz} orbitals.

The best theoretical RDF curve was obtained for **2b** (Figure 18) when a similar three-chain structural model shown in Figure

(35) Müller, A.; Krickemeyer, E.; Bögge, H.; Clegg, W.; Sheldrick, G. M. *Angew. Chem., Int. Ed. Engl.* **1983**, *22*, 1006–1007.

(36) Shibaeva, R. P. *Sov. Phys.-Crystallogr. (Engl. Transl.)* **1983**, *28*, 644–648.

(37) Kobayashi, H.; Kobayashi, A.; Saito, G.; Inokuchi, H. *Chem. Lett.* **1982**, 245–246.

(38) Alvarez, S.; Vicente, R.; Hoffmann, R. *J. Am. Chem. Soc.* **1985**, *107*, 6253–6277.

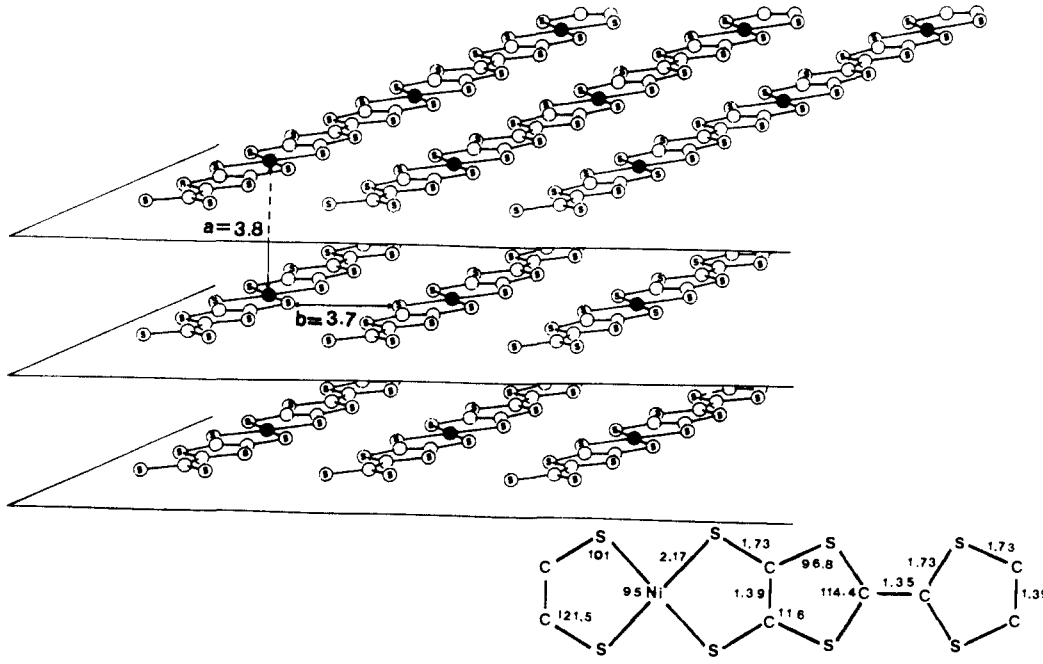

Figure 12. Nine-chain model of polymer **2a**. In this case, for the sake clarity, the planes each containing three coplanar parallel chains have been materialized. Distances are in Å and angles in deg.

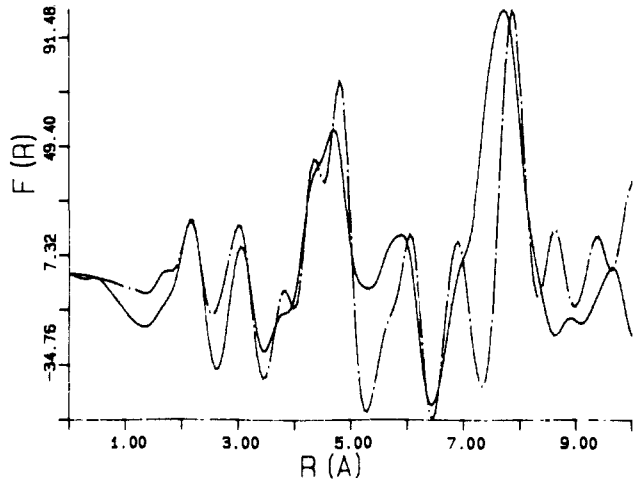

Figure 13. Experimental RDF curve of polymer **3** (—) and theoretical RDF curve (-·-) calculated by using the structural model of Figure 14.

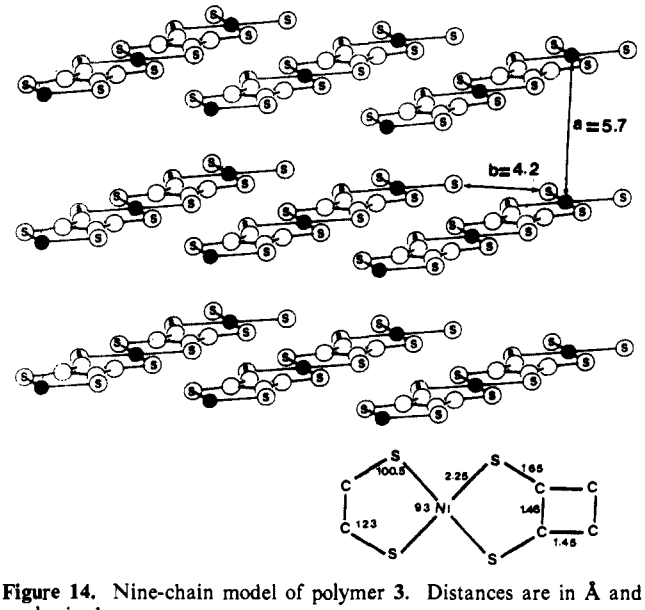

Figure 14. Nine-chain model of polymer **3**. Distances are in Å and angles in deg.

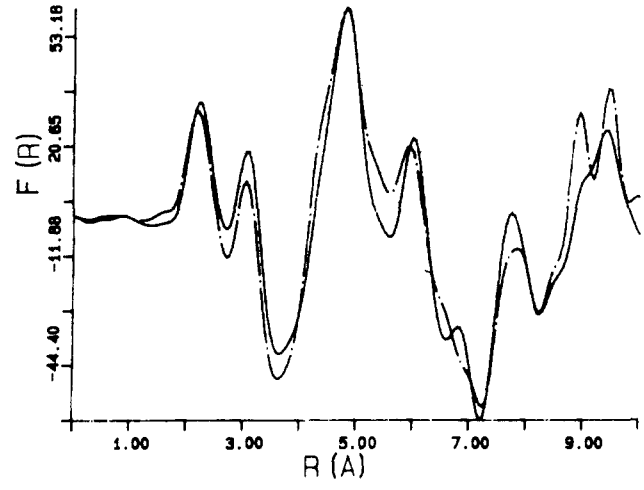

Figure 15. Experimental RDF curve of polymers **1c** (—) and **2b** (-·-).

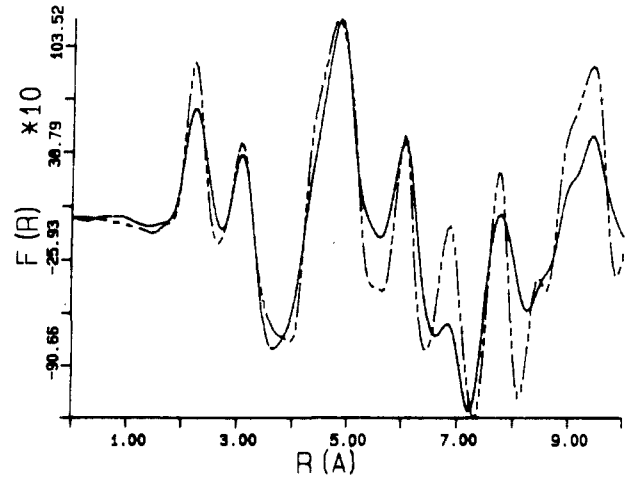

Figure 16. Experimental RDF curve of polymer **1c** (—) and theoretical RDF curve (---) calculated by using the structural model of Figure 17.

19 was used. In this case, the slipping effect observed in **1c** was not found again. This may be simply due to the larger number of geometrical parameters in the ttftt ligand which enter in much more complicated simulations, so that such a slipping cannot be

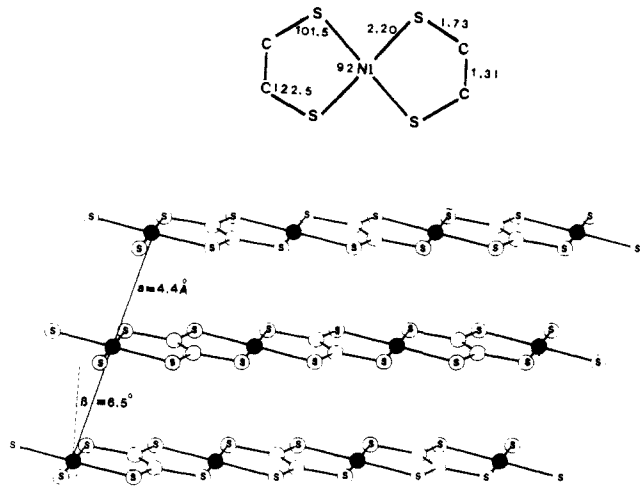

Figure 17. Three-chain model of polymer **1c**. Distances are in Å and angles in deg.

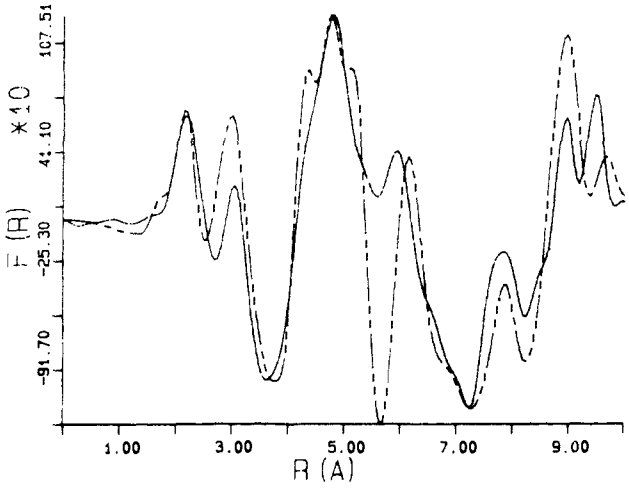

Figure 18. Experimental RDF curve of polymer **2b** (—) and theoretical RDF curve (---) calculated by using the structural model of Figure 19.

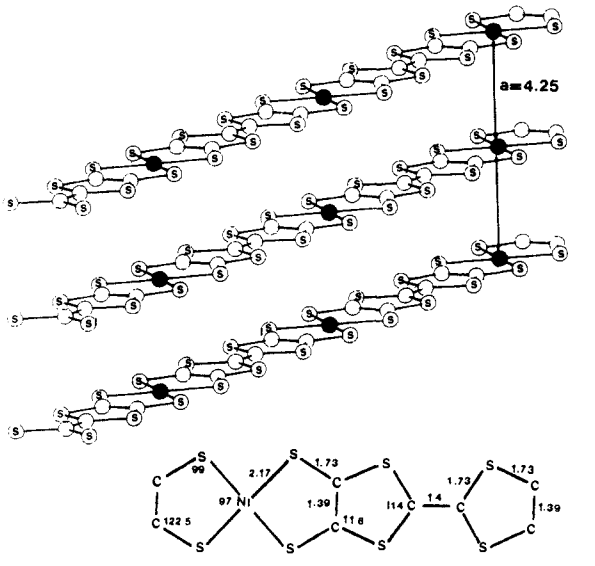

Figure 19. Three-chain model of polymer **2b**. Distances are in Å and angles in deg.

definitely ruled out in the case of **2b**.

It was expected that the RDF curve of polymer **1d** which has the bulky countercation $[Co(pmi)_2]^{2+}$ would look like those of polymers with large cations, i.e., **1c** or **2b**. Yet, the experimental RDF curve of **1d** (Figure 20) resembles more that of **1a** where the cation is Na^+. However, the first peak at ca. 2.2 Å shows

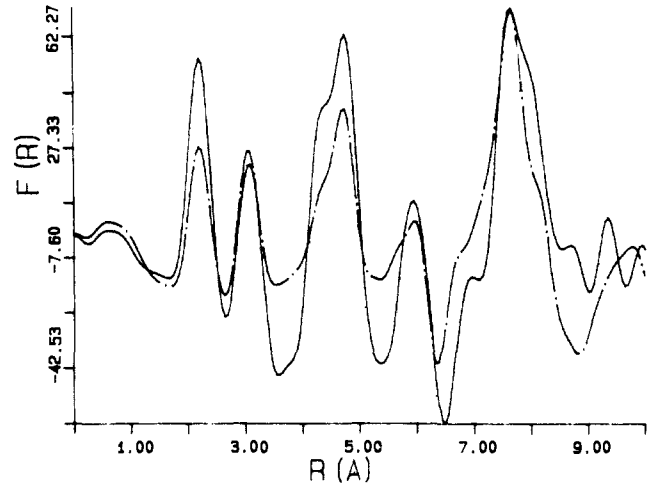

Figure 20. Comparison of the experimental RDF curves of polymers **1a** (—) and **1d** (-·-).

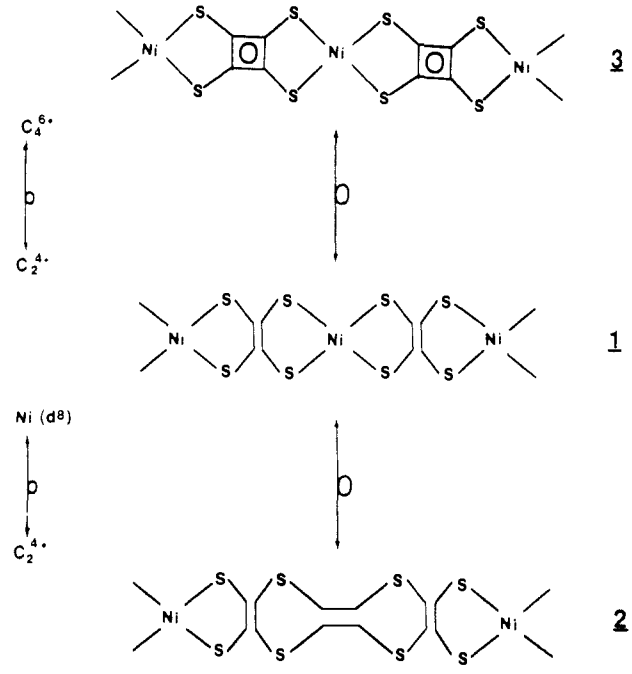

Figure 21. Isolobal analogies for polymers **1**, **2**, and **3**.

a much higher intensity in the case of **1d**. This is due to Co–N interactions of the $[Co(pmi)_2]^{2+}$ cation. Likewise, the intensity increase of the peak at ca. 4.5 Å is probably due to interactions within the $[Co(pmi)_2]^{2+}$ cation. Attempts to locate the $[Co(pmi)_2]^{2+}$ cations in **1d** have failed so far.[15]

Discussion

The first observation that can be made upon comparison of the RDF curves and corresponding structural models derived from LAXS studies is that the studied polymers exhibit two types of short- and middle-range order (SMRO) in their structural arrangement. The polymers with Na^+, K^+, and $[Co(pmi)_2]^{2+}$ cations exhibit SMRO we call of type I, which may be described by the nine-chain models shown in Figures 7, 12, and 14. Those with the n-Bu_4N^+ cation exhibit SMRO of type II, which may be described by the three-chain models shown in Figures 17 and 19.

A noticeable point is that the SMRO-type polymer only depends on the nature of the countercation and not on that of the ligand. In a recent paper, Hoffmann et al.[38] pointed out the isolobal analogy of a metal d^8 (Ni^{2+}) fragment with the ethylene (C_2^{4+}) and squarate (C_4^{6+}) fragments. Following this concept, replacing every other Ni^{2+} ion in the (Ni-ett) polymers **1** by its isolobal analogue C_2^{4+} will lead to the (Ni-ttftt) polymers **2** (Figure 21). Likewise, replacing each C_2^{4+} fragment in polymers **1** by its

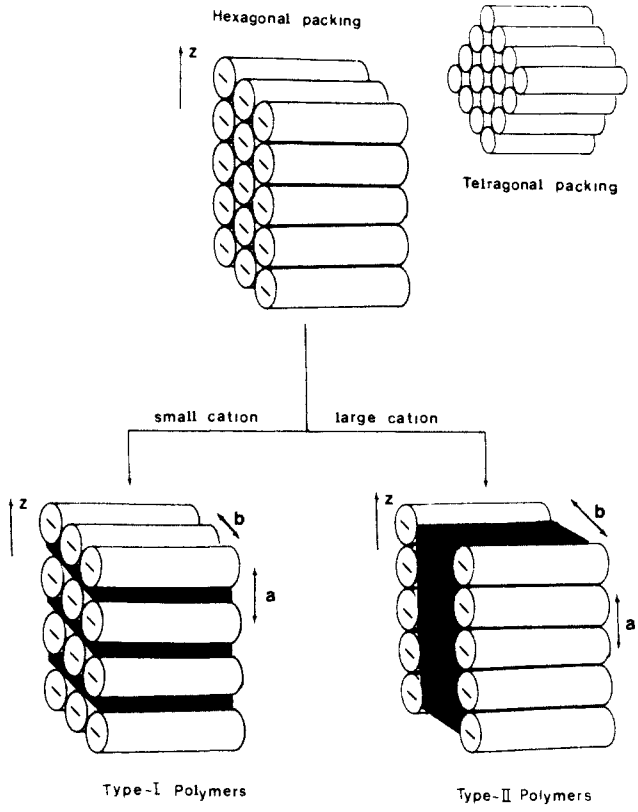

Figure 22. Hexagonal (honeycomb) and tetragonal packings of parallel cylinders.[39] SMRO type I and type II structural arrangements derived from the hexagonal packing.[41] The slit into the base of the cylinders represents the polymer-chain plane.

isolobal analogue C_4^{6+} will lead to the (Ni-tts) polymers **3**.

The classification of the studied polymers into SMRO-type I and SMRO-type II may be rationalized by using the description of rod packing as described by O'Keefe and Andersson.[39] In this description, the crystallographic packing is represented by uniform cylinders instead of spheres as usual. Figure 22 represents the two simplest packings, the hexagonal (honeycomb) and the tetragonal packing. For example, Strähle and Fuchs[40] have shown that in scandium(III) acetate, the polymeric columns of scandium atoms, which are connected by three bridging acetato groups, are arranged in an ideal hexagonal close packing of cylindrical rods.

As the single chain in the studied polymers is roughly planar, at least in a short range, we may enrich the rod packing description by assuming that the single chains are stacked perpendicularly to an arbitrary axis, z. This is represented in Figure 22 by the slit onto the base of the cylinders. Starting from the hexagonal packing,[41] and intercalating between the rods black layers perpendicular to the z axis as a location for the cations Na^+, K^+, or $[Co(pmi)_2]^{2+}$, we get a structural arrangement of type I which resembles the nine-chain structural models obtained for the corresponding polymers **1a**, **1b**, **1d**, **2a**, and **3** (Figures 7, 12, and 14). On the other hand, starting from the same original packing and intercalating black layers parallel to the z axis as a location for the n-Bu_4N^+ cation, we get a structural arrangement of type II which resembles the models obtained for polymers **1c** and **2b** (Figures 17 and 19).

(39) O'Keeffe, M.; Andersson, S. *Acta Crystallogr., Sect. A* **1977**, *A33*, 914–923.

(40) Fuchs, R.; Strähle, J. *Z. Naturforsch.* **1984**, *39b*, 1662–1663.

(41) Similar type-I and type-II structural arrangements could be derived by the same procedure starting from the tetragonal packing.

Table II. Specific Weight ρ ($g \cdot cm^{-3}$), SMRO-Type and Parameters a and b (Å), and Conductivity ($\Omega^{-1} \cdot cm^{-1}$) of the Studied Polymers

polymer	ligand	cation	SRO-type	ρ	a	b	σ
1a	ett	Na^+	I	2.11	4.55	4.33	4
1c	ett	n-Bu_4N^+	II	1.72	4.4	>10	10^{-2}
2a	ttftt	Na^+	I	2.00	3.8	3.7	5
2b	ttftt	n-Bu_4N^+	II	1.47	4.3	>10	10^{-4}
3	tts	Na^+	I	2.12	5.7	4.2	10^{-4}

As shown by the a and b values listed in Table II, the type I polymers have a packing that is closer to the original hexagonal (or tetragonal) packing than the packing of the type II polymers. It is difficult to ascertain the effects of a perturbation of an original packing on the energy state of the system and it may be likewise speculated upon the possible contributing factors for cation placement in the structure, such as cation size, charge, and binding potential. Nevertheless, given the values of the a and b parameters and of the specific weight ρ, one possible explanation could be that by introducing countercations the original packing may tend to resist the structural perturbation and try to achieve the densest packing with a minimum of energy and a maximum of symmetry. With this assumption, the introduction of small cations such as Na^+, K^+, or a flat complex cation, as $[Co(pmi)_2]^{2+}$ probably is, causes a smaller structural distortion than the introduction of a bulky cation such as n-Bu_4N^+. As a consequence, the densities of type II polymers should be lower than those of type I polymers. This is consistent with the values, listed in Table II, of the densities of the polymers.

In type I polymers, there are two kinds of interchain interactions: (i) those parallel to the stacking axis z corresponding to the a parameter (3.7–5.7 Å, Table II), and (ii) side-by-side interactions perpendicular to z corresponding to the b parameter (3.8–4.5 Å). On the other hand, in type II polymers, the b type interchain interactions no longer exist since the stacked chains are separated by the n-Bu_4N^+ layers and are further than 10 Å from each other, but interchain interactions along the stacking axis z are still observed and correspond to a values of 4.3–4.4 Å. This difference in the interchain interactions should also be correlated to the values of the compaction powder conductivities of the corresponding polymers (Table II). As a matter of fact, the conductivities of **1a** and **2a** (type I) are more than two orders of magnitude higher than the conductivities of **1c** and **2b** (type II), respectively. This result suggests that the interstack (side-by-side) interactions are as important as the intrastack interactions in determining the electrical properties of these polymers. Noteworthy is that a similar observation has been made in the case of conductive BEDT-TTF-based molecular compounds[2,42] and $M(dmit)_2$ complexes.[2,35] The low conductivity observed for type I polymer **3** is probably related to the large intrastack a value (5.7 Å).

Acknowledgment. We thank J. Aussoleil for his programming skills, turning the LASIP system into the "TURBO" version. We also thank J. Ribas and R. Vicente for sharing their expertise in the synthesis of the studied polymers and J. Strähle for helpful discussion about the structural determination presented in this work.

(42) (a) Saito, G.; Enoki, T.; Toriumi, K.; Inokuchi, H. *Solid State Commun.* **1982**, *42*, 557–560. (b) Kaminski, V. F.; Prokhorova, T. G.; Shibaeva, R. P.; Yagubskii, E. B. *Pis'ma Zh. Eksp. Teor. Fiz.* **1984**, *39*, 15–18 (*JETP Lett. (Engl. Transl.)* **1984**, *39*, 17–20). (c) Kobayashi, H.; Kobayashi, A.; Sasaki, Y.; Saito, G.; Enoki, T.; Inokuchi, H. *J. Am. Chem. Soc.* **1983**, *105*, 297–298. (d) Williams, J. M.; Wang, H. H.; Beno, M. A.; Emge, T. J.; Sowa, L. M.; Copps, P. T.; Behroozi, F.; Hall, L. N.; Carlson, K. D.; Crabtree, G. W. *Inorg. Chem.* **1984**, *23*, 3839–3841. (e) Williams, J. M.; Beno, M. A.; Wang, H. H.; Reed, P. E.; Azevedo, L. J.; Schriber, J. E. *Inorg. Chem.* **1984**, *23*, 1790–1792.